

See discussions, stats, and author profiles for this publication at: <https://www.researchgate.net/publication/231647942>

Morphological and Structural Changes during the Reduction and Reoxidation of CuO/CeO₂ and Ce_{1-x}Cu_xO₂ Nanocatalysts: In Situ Studies with Environmental TEM, XRD, and XAS

ARTICLE *in* THE JOURNAL OF PHYSICAL CHEMISTRY C · JUNE 2011

Impact Factor: 4.77 · DOI: 10.1021/jp203882h

CITATIONS

30

READS

64

7 AUTHORS, INCLUDING:



Jonathan Hanson

Brookhaven National Laboratory

174 PUBLICATIONS 6,734 CITATIONS

[SEE PROFILE](#)



Marcos Fernández-García

Spanish National Research Council

258 PUBLICATIONS 8,515 CITATIONS

[SEE PROFILE](#)

Morphological and Structural Changes during the Reduction and Reoxidation of CuO/CeO₂ and Ce_{1-x}Cu_xO₂ Nanocatalysts: *In Situ* Studies with Environmental TEM, XRD, and XAS

James Ciston,[†] Rui Si,[‡] Jose A. Rodriguez,^{*‡} Jonathan C. Hanson,[‡] Arturo Martínez-Arias,[§] Marcos Fernandez-García,[§] and Yimei Zhu^{†,⊥}

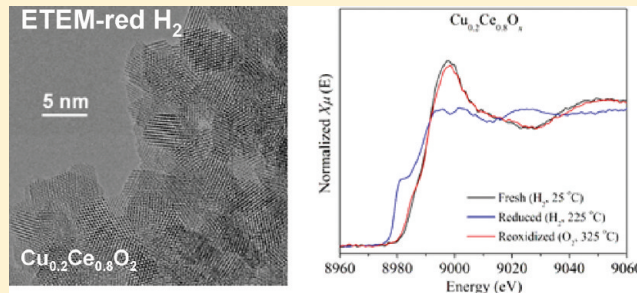
[†]Center for Functional Nanomaterials, Brookhaven National Laboratory, Upton, New York 11973, United States

[‡]Department of Chemistry, Brookhaven National Laboratory, Upton, New York 11973, United States

[§]Instituto de Catálisis y Petroleoquímica, CSIC, Campus Cantoblanco, 28049 Madrid, Spain

[⊥]Department of Condensed Matter Physics and Materials Science, Brookhaven National Laboratory, Upton, New York 11973, United States

ABSTRACT: We have studied the structural, morphological, and electronic properties of CuO/CeO₂ and Ce_{1-x}Cu_xO₂ nanocatalysts during reduction/oxidation cycles using H₂ and O₂ as chemical probes. Time-resolved *in situ* characterization was performed by X-ray diffraction (XRD) and X-ray absorption spectroscopy (XAS) as well as aberration-corrected environmental transmission electron microscopy (ETEM). We have found that both types of nanocatalysts reduce to a Cu/CeO₂ biphase system with significant oxygen vacancies in CeO₂. Important variations are seen in the Cu particle size and metal dispersion depending on the initial state of the copper oxide–ceria systems. During subsequent *in situ* oxygen annealing, the Cu precipitated from the CuO/CeO₂ system reoxidized to form CuO through a Cu₂O intermediate phase as expected. However, the Cu precipitated from the Ce_{0.8}Cu_{0.2}O₂ solid solution behaved rather differently under oxidizing conditions, and neither oxidized to form CuO nor fully returned to a bulk Ce_{0.8}Cu_{0.2}O₂ phase in solid solution. We found that ~50% of the Cu returned to a Ce_{1-x}Cu_xO₂ solid solution, while the remainder was observed by *in situ* ETEM to form an amorphous copper oxide phase with a Cu oxidation state similar to Ce_{1-x}Cu_xO₂, but with a local bonding environment similar to CuO. The behavior of the reduced Ce_{0.8}Cu_{0.2}O₂ reflects strong interactions between Cu and the ceria matrix and illustrates the advantages of working with solid solutions of mixed oxides.



INTRODUCTION

The rarity of noble metal catalysts presents serious hurdles to the implementation of clean energy technologies on a global scale.¹ However, catalytic materials based on the copper oxide framework are promising as more economical alternatives.^{1–3} Copper oxide is used as a catalyst or catalyst precursor in many chemical reactions that involve hydrogen as a reactant or a product: methanol synthesis from CO (CO + 2H₂ → CH₃OH) or CO₂ (CO₂ + 3H₂ → CH₃OH + H₂O),^{2,4} the water-gas shift reaction (CO + H₂O → CO₂ + H₂),^{2,5,6} methanol steam reforming (CH₃OH + H₂O → CO₂ + 3H₂),^{2,7} oxidative methanol reforming (CH₃OH + 1/4O₂ + 1/2H₂O → CO₂ + 5/2H₂),⁸ NO reduction (NO + H₂ → 1/2N₂ + H₂O),^{2,9} etc. It has been proposed that in several of these catalytic processes the CuO precursor undergoes reduction and Cu¹⁺ or Cu⁰ (i.e., metallic copper) is the real active phase.^{2,5,6,10} CuO, Cu₄O₃, and Cu₂O are well-known copper oxides with monoclinic, tetragonal, and cubic crystal structures, respectively.^{11–14} Thermodynamically, the oxidation state of copper changes among CuO, Cu₂O, and Cu as a function of temperature and oxygen

partial pressure.^{15,16} The relative stability of the Cu²⁺, Cu¹⁺, and Cu⁰ species can change when one has mixtures of copper oxide and another oxide.^{2,10,17,18} In spite of the tremendous amount of work carried out to explore the nature of the active sites of copper-oxide based catalysts (CuO, CuO/ZnO, CuO/CeO₂, CuO/ZrCeO₄, CuAl₂O₄, and CuCr₂O₄ spinels, etc.) under reducing environments,^{19–27} the morphological and structural changes in the presence of H₂ have not been correlated through *in situ* studies.

In this work, we investigate the reduction and reoxidation of two different precursors of CuO–CeO₂ catalysts: Ce_{0.8}Cu_{0.2}O₂ solid solutions with the copper dopant fully incorporated into the fluorite structure²⁸ and CuO/CeO₂ blends in which copper oxide is just impregnated on a ceria substrate. Both types of CuO–CeO₂ catalysts have shown very good activity for water-gas shift and oxidation of CO.^{23,27} While it has been

Received: April 26, 2011

Revised: June 3, 2011

Published: June 08, 2011

established that CuO/CeO₂ blends yield significantly higher catalytic activities than CeO₂ alone, the nature of this enhancement is complex due to the flexible valence of both Cu and Ce, leading to a variable oxygen storage capacity within their native and mixed oxides.^{29–32} Consequently, catalytic activity for a given reaction depends strongly upon the precursor and its activation, with Ce_{1-x}Cu_xO₂ exhibiting superior performance for CO oxidation³³ and CuO/CeO₂ blends yielding a somewhat higher activity for the water-gas shift reaction.²⁸ In the past, the structural and electronic properties of Ce_{1-x}Cu_xO₂ nanocatalysts have been studied using a combination of synchrotron-based X-ray diffraction (XRD), X-ray absorption spectroscopy (XAS), Raman spectroscopy, and density functional calculations.³⁴ These studies showed that the Ce_{1-x}Cu_xO₂ systems are indeed solid solutions.³⁴ The copper atoms embedded in ceria had an oxidation state higher than those of the cations in Cu₂O or CuO. The lattice of the Ce_{1-x}Cu_xO₂ systems still adopted a fluorite-type structure but was highly distorted with multiple cation–oxygen distances with respect to the single cation–oxygen bond length seen in pure ceria.³⁴ There was a cell dimension decrease when the Cu went into the ceria and a cell dimension increase when the Cu came out. The doping of CeO₂ with copper introduced a large strain into the oxide lattice and favored the formation of O vacancies. Cu approached the planar geometry characteristic of Cu²⁺ oxides but with a strongly perturbed local order.³⁴ The chemical activities of the Ce_{1-x}Cu_xO₂ nanoparticles were tested using the reactions with H₂, CO, and O₂ as probes.³⁴ During the reduction in hydrogen, an induction time was observed and became shorter after raising the reaction temperature. The fraction of copper that could be reduced in the Ce_{1-x}Cu_xO₂ solid solutions also depended strongly on the reaction temperature.³⁴ A comparison with data for the reduction of pure copper oxides indicated that the copper embedded in ceria was much more difficult to reduce.

Here, the structural and electronic properties of Ce_{0.8}Cu_{0.2}O₂ and CuO/CeO₂ under an atmosphere of H₂ were studied in detail using synchrotron-based time-resolved *in situ* XRD and XAS to assess the ensemble average properties. Aberration-corrected environmental transmission electron microscopy (ETEM) was also used to elucidate single particle behavior at the atomic scale and to identify morphological changes in the surface of the catalysts. Important differences are observed in the structural/morphological properties of Ce_{0.8}Cu_{0.2}O₂ and CuO/CeO₂ during reduction/reoxidation processes. In the case of the reduced Ce_{0.8}Cu_{0.2}O₂ solid solution, the strong interaction between copper and the ceria matrix produced a distinctive behavior not seen for a simple blend of the oxides (CuO/CeO₂).

METHODS

A. Sample Preparation. The reference CuO, Cu₂O, and Cu bulk samples used in this work were obtained from commercial sources (>99.99% purity). Cu-doped ceria, labeled as Ce_{0.8}-Cu_{0.2}O₂, was prepared with a modified reverse microemulsion method.^{23,35–37} Briefly, the precursors were introduced in a reverse microemulsion (water in oil) using *n*-heptane as the organic phase, Triton X-100 (Aldrich) as surfactant, and hexanol as cosurfactant. Then, this suspension was mixed with another similar suspension containing as aqueous phase in alkali solution (trimethylanilinium hydroxide (TMAH), Aldrich). All cations were coprecipitated, and the resulting mixture was stirred for 24 h, centrifuged, decanted, and rinsed with methanol. Finally, the

solid portion was dried overnight at 100 °C, and the resulting powder was calcined under air at 500 °C for 2 h. ICP-AES chemical analysis of this type of sample confirmed quantitative precipitation of both Cu and Ce cations.

The sample of copper oxide supported on CeO₂ (Cu wt % of 5, denoted hereafter as CuO/CeO₂) was prepared by incipient wetness impregnation of a CeO₂ support synthesized by micro-emulsion (in a similar manner as described above) with copper nitrate aqueous solutions. Following impregnation, the sample was dried overnight at 100 °C and finally calcined under air at 500 °C for 2 h.

B. Time-Resolved X-ray Diffraction. The time-resolved X-ray diffraction experiments were carried out on beamline X7B ($\lambda = 0.3184 \text{ \AA}$) of the National Synchrotron Light Source (NSLS) at Brookhaven National Laboratory (BNL). The powder sample (~3 mg) was loaded into a glass capillary cell (i.D. = 0.8 mm) which was attached to a flow system.³⁸ A small resistance heating wire was installed right below the capillary, and the temperature was monitored with a 0.5 mm chromel–alumel thermocouple that was placed in the capillary near the sample. *In situ* diffraction patterns were collected during reduction (5% H₂/He) and reoxidation (5% O₂/He) under a ramping mode with a heating rate of 4 °C/min at a flow rate of 10 mL/min. A Perkin-Elmer detector was used to record X-ray patterns. Two-dimensional powder patterns were collected with an image-plate detector, and the powder rings were integrated using the FIT2D code.³⁹ Phase diagrams for CuO, Cu₂O, Cu, and CeO₂ and the lattice constants of ceria were calculated through Rietveld refinement.⁴⁰ The molar fraction was equal to $M_n / (M_{\text{CuO}} + M_{\text{Cu}_2\text{O}} + M_{\text{Cu}} + M_{\text{Cu in ceria}} + M_{\text{Ce in ceria}})$, and the M_n is the amount (unit: moles) of each metal/metal oxide species and was determined by Rietveld refinement.

C. X-ray Absorption Spectroscopy. Cu K absorption edge ($E_0 = 8979 \text{ eV}$) XAFS spectra were collected *in situ* at beamline X18B of the NSLS at BNL during the reduction and reoxidation of the catalysts under similar conditions as the XRD experiments with the exception of the gas mixture used for the reoxidation (20% O₂/He). A commercially available Kapton cell (o.d. = $1/8 \text{ in.}$) was used for mounting the sample (~50 mg). An air-flow heating gun with temperature controller was used to heat the powder samples with a ramping rate of 2 °C/min for reduction and 5 °C/min for reoxidation. The X-ray absorption spectra were taken repeatedly in the “fluorescence-yield mode” using a Pips (passivated-implanted planar silicon) detector cooled with circulating water. The energy was calibrated for each scan with the first inflection point of the Cu K edge in Cu metal foil. The EXAFS data have been analyzed using the Athena and Artimis programs.⁴¹

D. Environmental Transmission Electron Microscopy. ETEM measurements were carried out on the FEI Titan 80-300 microscope at the Center for Functional Nanomaterials, Brookhaven National Laboratory. This instrument is equipped with a differentially pumped environmental cell capable of 10 Torr gas injection and a CEOS postobjective geometric image aberration corrector. HRTEM imaging was carried out at 300 kV with the aberration corrector tuned to a flat phase region of >20 mrad (third-order aberration correction and <0.1 nm information transfer), with residual spherical aberration <1.5 μm. Transmission electron diffraction (TED) data were collected using a parallel 100 nm beam without selected area aperture. The as-prepared ETEM samples were supported on a porous amorphous SiN grids (PELCO 200 nm SiN with 2.5 μm pores).

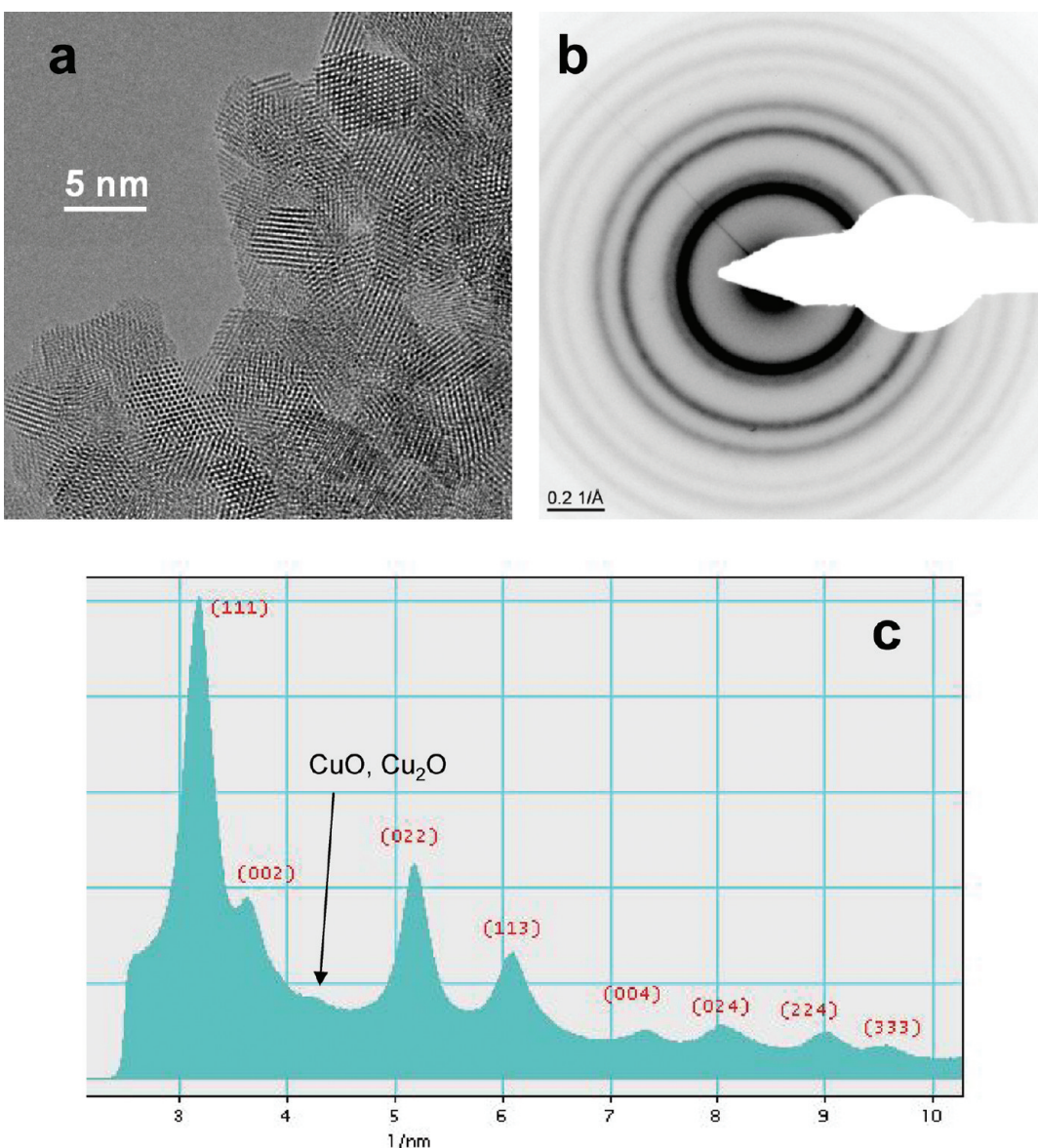


Figure 1. (a) HREM image of as-prepared Ce_{0.8}Cu_{0.2}O₂ particles at 30 °C in 10⁻⁷ Torr vacuum. (b, c) Electron diffraction patterns of Ce_{0.8}Cu_{0.2}O₂ showing mainly CeO₂-type features with a weak peak that could correspond to CuO or Cu₂O.

The samples were heated to 400 at 20 °C/min in 1.5 Torr of either H₂ or O₂ using a Gatan 652 heating holder with an Inconel furnace.

RESULTS AND DISCUSSION

A. In Situ Environmental TEM Studies. We performed *in situ* time-resolved ETEM experiments for the Ce_{0.8}Cu_{0.2}O₂ and CuO/CeO₂ samples under both reducing and oxidizing environments to elucidate their behavior at the single particle level and to follow variations in the surface morphology of these nanocatalysts. The as-prepared Ce_{1-x}Cu_xO₂ particles had an average size of 4.64 ± 0.95 nm and often exhibited faceted terminations without amorphous edges (Figure 1a). Electron diffraction (ED) data were collected (Figure 1b) and showed nearly pure CeO₂-type reflections, with a minor amount of a CuO or Cu₂O phase present (Figure 1c). Results of XRD, to be discussed below, also indicated that the amount of CuO_x present in the Ce_{0.8}Cu_{0.2}O₂

sample was small (~0.04 molar fraction). In Figure 1, there is no indication of an ordered Cu sublattice in the Ce_{0.8}Cu_{0.2}O₂ from either HREM imaging or diffraction. All the features seen point to a typical fluorite lattice for the Ce_{0.8}Cu_{0.2}O₂ sample. The copper embedded inside the ceria does induce a change in the cell parameter, introduces stress in the lattice, and produces O vacancies,^{27,33} but the main surface morphological features of the Ce_{0.8}Cu_{0.2}O₂ solid solution are similar to those of pure CeO₂.

The Ce_{0.8}Cu_{0.2}O₂ was exposed to 1.5 Torr of H₂ to induce the reduction of copper.^{27,33} Upon heating the sample rapidly to 400 °C, CuO_x reflections briefly became more pronounced (not shown) before disappearing entirely after 10 min, leaving only CeO₂ and Cu reflections in the ED pattern (Figure 2a). After 60 min of reduction, Cu reflections increased in intensity, while the average CeO₂ particle size dropped from 4.64 ± 0.95 to 4.36 ± 0.46 nm, indicating an 18% loss of volume due to Cu diffusion from the bulk. The size of the Cu particles observed in

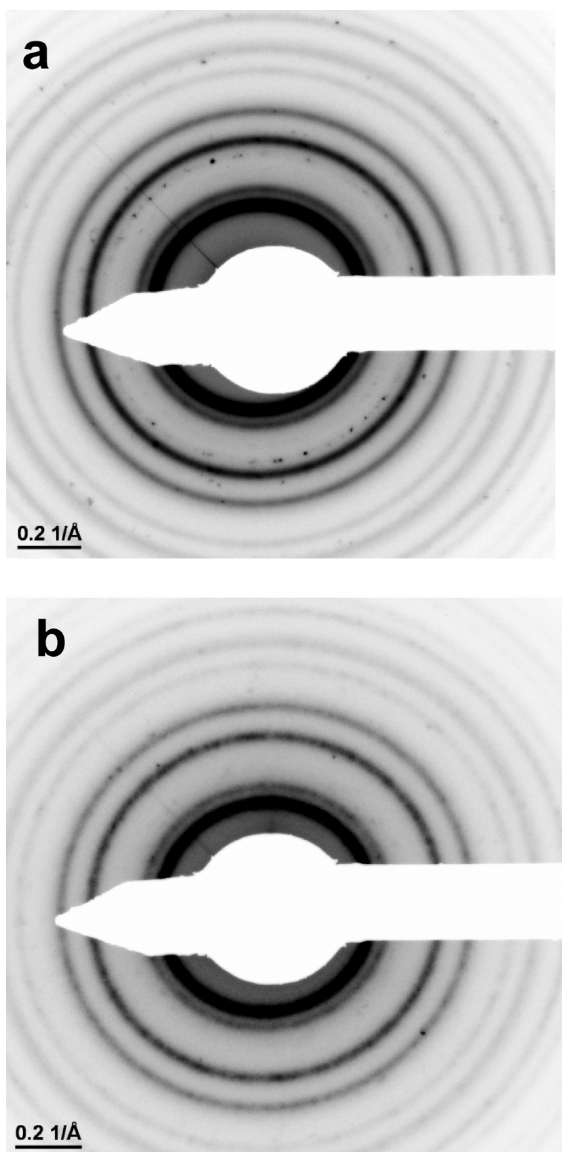


Figure 2. Electron diffraction patterns of $\text{Ce}_{0.8}\text{Cu}_{0.2}\text{O}_2$ (a) during H_2 anneal ($400\text{ }^\circ\text{C}$, 1.5 Torr) where additional Cu precipitate reflections have appeared and (b) during O_2 anneal ($400\text{ }^\circ\text{C}$, 1.5 Torr) where Cu reflections have vanished, leaving only CeO_2 -type rings.

TEM was 10 nm, larger than anticipated, and indicative of Ostwald ripening. The existence of smaller Cu particles ($<1\text{ nm}$) dispersed on the ceria support cannot be ruled out, as these poorly crystalline particles would not be detected during an ETEM experiment at these pressures. The CeO_2 particles remained highly crystalline under these conditions with an absence of amorphous material at the edge as displayed in Figure 3a. From measurements of X-ray absorption spectroscopy (see below), one can conclude that at $400\text{ }^\circ\text{C}$ all the copper has been reduced by hydrogen and removed from the oxide matrix, and there is also some reduction of the cerium cations ($\text{Ce}^{4+} \rightarrow \text{Ce}^{3+}$). These important changes do not seem to affect the main structural and morphological features of the ceria. After reduction of $\text{Ce}_{0.8}\text{Cu}_{0.2}\text{O}_2$ in H_2 , the system contains Cu nanoparticles dispersed on a well-defined ceria substrate that mostly exhibits $\{111\}$ facets.

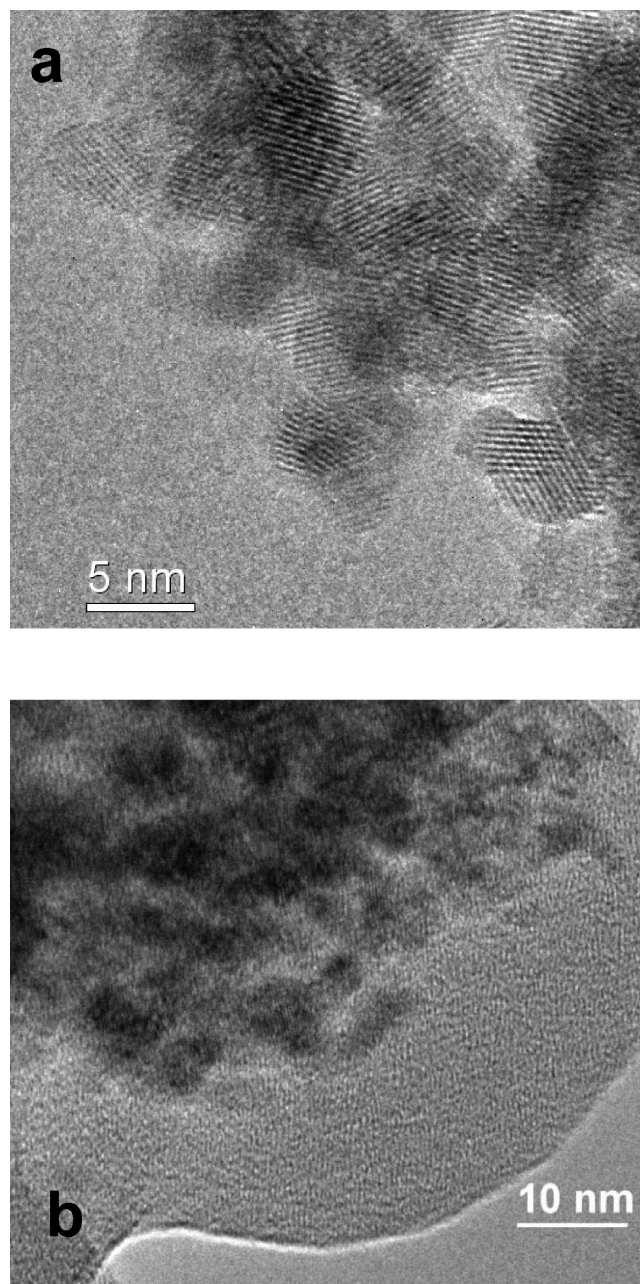


Figure 3. HREM image of (a) $\text{Ce}_{0.8}\text{Cu}_{0.2}\text{O}_2$ after 60 min reduction at $400\text{ }^\circ\text{C}$ in 1.5 Torr of H_2 (image recorded at $350\text{ }^\circ\text{C}$ in 0.25 Torr of H_2) and (b) after subsequent reoxidation at $400\text{ }^\circ\text{C}$ in O_2 (image recorded at $30\text{ }^\circ\text{C}$ in 1 Torr of O_2).

The sample in Figure 3a was then cooled to room temperature under 1.5 Torr of H_2 , pumped to vacuum, and heated *in situ* to $400\text{ }^\circ\text{C}$ under 1.5 Torr of O_2 . After 15 min of oxidation, Cu reflections were no longer detected by electron diffraction leaving only CeO_2 -type rings. However, an amorphous phase had grown on the CeO_2 particle surface, reaching 10 nm thick in some regions (Figure 3b) while other regions exhibited minimal amorphous growth. This phase was confirmed by electron energy-loss spectroscopy (EELS) to be a carbon-free amorphous oxide. We propose that after Ostwald ripening of the precipitated Cu phase, oxidation causes the smaller residual Cu particles to be reincorporated into the

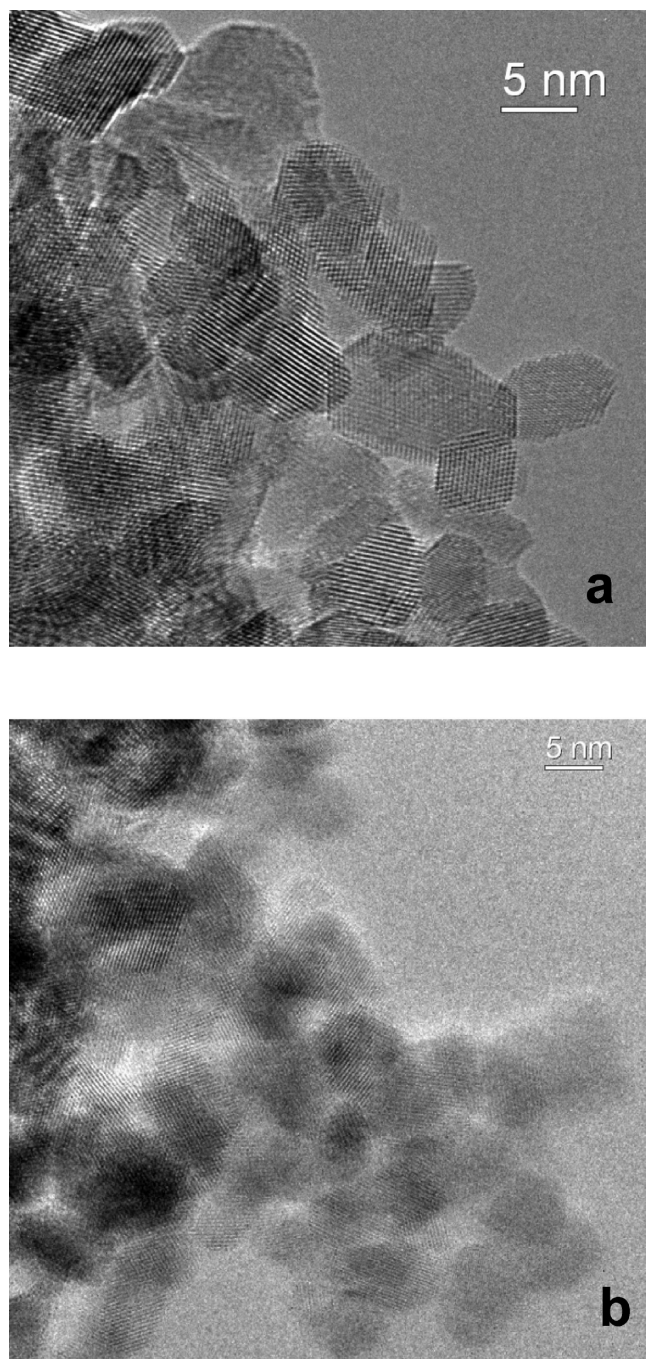


Figure 4. HREM image of (a) as-prepared CuO/CeO_2 particles at 30 $^{\circ}\text{C}$ in 10^{-7} Torr vacuum and (b) during oxidation at 400 $^{\circ}\text{C}$ in 1.3 Torr of O_2 , which followed a prior 60 min reduction at 400 $^{\circ}\text{C}$ in 1.5 Torr of H_2 .

CeO_2 matrix, while the larger 10 nm Cu particles form an amorphous oxide. In any case, strong interactions between the Cu and oxide phases produced by the reduction of $\text{Ce}_{0.8}\text{Cu}_{0.2}\text{O}_2$ apparently prevent the formation of a simple CuO/CeO_2 blend in which the reoxidized copper adopts the normal properties of a copper oxide. In the next section, we will use XRD to determine the amount of copper that returns into the ceria host upon reaction of O_2 with reduced $\text{Ce}_{0.8}\text{Cu}_{0.2}\text{O}_2$.

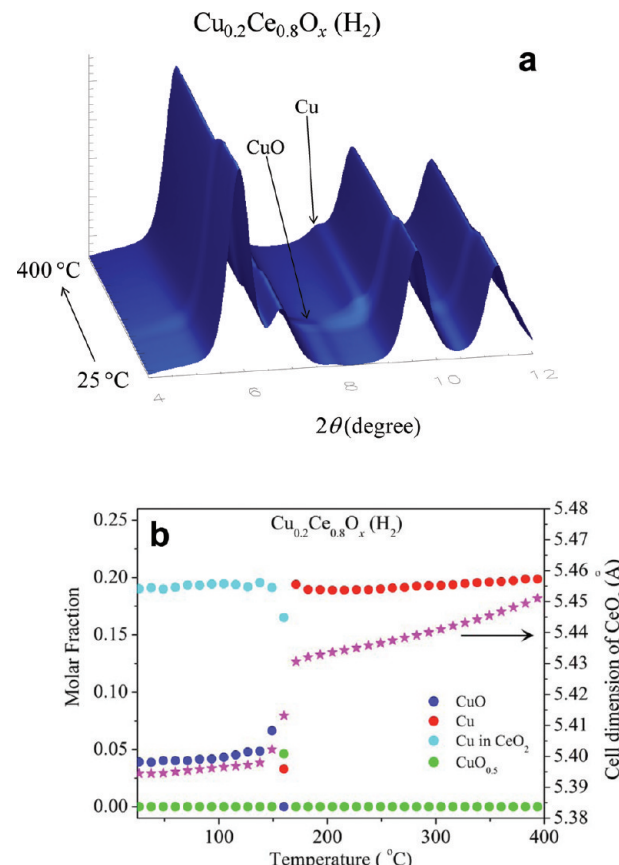


Figure 5. (a) *In situ* X-ray diffraction patterns collected during the heating of $\text{Ce}_{0.8}\text{Cu}_{0.2}\text{O}_2$ in 5% H_2/He from 25 to 400 $^{\circ}\text{C}$ at a heating rate of 4 $^{\circ}\text{C}/\text{min}$. (b) Results of a Rietveld refinement for the *in situ* time-resolved XRD data. Cu content is plotted as the molar fraction of the Cu + Ce total.

Figure 4a shows a TEM image for a 5% CuO/CeO_2 system prepared by standard impregnation of ceria with copper nitrate and subsequent calcination in air at elevated temperature (see Methods section). In this material, the crystalline CuO phase is less evenly distributed compared to the residual CuO in $\text{Ce}_{0.8}\text{Cu}_{0.2}\text{O}_2$. By repeating the full *in situ* ETEM study, we found that this CuO/CeO_2 blend could undergo cycles of reduction and oxidation without the deposition of an amorphous copper oxide on the ceria support. However, full reduction to metallic copper was only achieved for this sample after 60 min at 400 $^{\circ}\text{C}$. The copper oxide produced by *in situ* reoxidation in O_2 of the reduced CuO/CeO_2 was crystalline (Figure 4b), indicating that amorphous copper oxide is a unique product of the oxidation of reduced $\text{Ce}_{0.8}\text{Cu}_{0.2}\text{O}_2$. This may be of great importance in catalytic applications where amorphous CuO is expected to be more active than crystalline CuO .^{2,5,16}

B. *In Situ* XRD Studies. *In situ* time-resolved X-ray diffraction patterns were collected for the $\text{Ce}_{0.8}\text{Cu}_{0.2}\text{O}_2$ and 5% CuO/CeO_2 samples during reduction and oxidation experiments. Figure 5 displays XRD data for the reduction of $\text{Ce}_{0.8}\text{Cu}_{0.2}\text{O}_2$. In agreement with the electron diffraction data in Figure 1, the XRD measurements show that initially the system exhibits the fluorite features with a small peak for CuO . In the bottom of Figure 5, we can see the results of a Rietveld refinement of the XRD data for the heating of $\text{Ce}_{0.8}\text{Cu}_{0.2}\text{O}_2$ in 5% H_2/He . At room temperature,

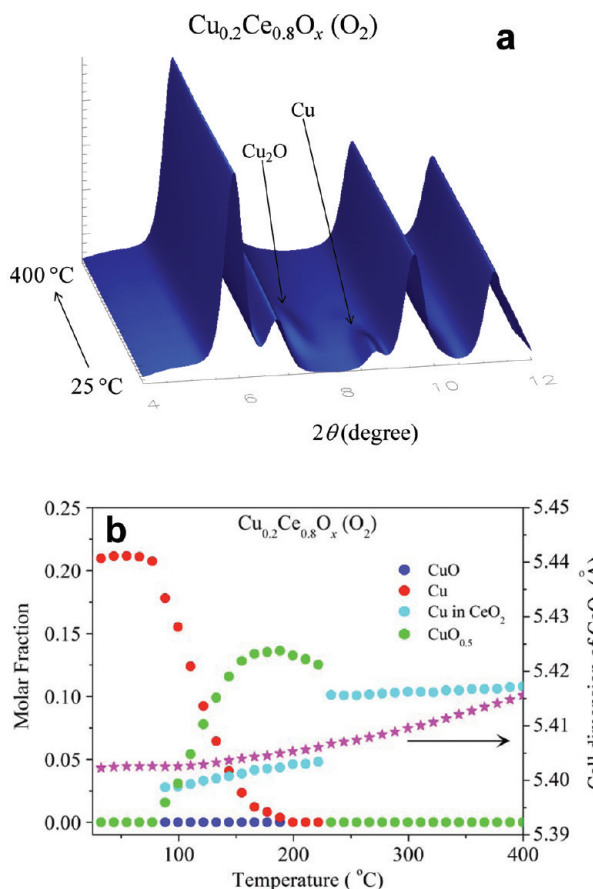


Figure 6. (a) *In situ* X-ray diffraction patterns collected during the reoxidation of reduced $\text{Ce}_{0.8}\text{Cu}_{0.2}\text{O}_2$ in 5% O_2/He from 25 to 400 °C at a heating rate of 4 °C/min. (b) Results of a Rietveld refinement for the *in situ* time-resolved XRD data. Cu content is plotted as the molar fraction of the Cu + Ce total.

the $\text{Ce}_{0.8}\text{Cu}_{0.2}\text{O}_2$ phase has a Cu:Ce molar ratio of 0.25 (0.19:0.77, calculated on the basis of the data in Figure 5b), with ~25% of the available Cu in a CuO impurity phase. At 160 °C, the Cu dopant is rapidly and entirely expelled from the $\text{Ce}_{0.8}\text{Cu}_{0.2}\text{O}_2$ solid solution and reduced to metallic Cu. This is accompanied by a discontinuous increase (~0.03 Å) in the CeO_2 lattice parameter indicative of rapid vacancy generation. This increase could reflect the removal of copper from the oxide matrix or the partial reduction of ceria (Ce^{4+} has a larger atomic size than Ce^{4+}).^{27,33} Simultaneously, the CuO impurity phase is reduced to form Cu_2O , which becomes difficult to refine in powder diffraction due to peak overlap with Cu at 8.7° 2θ and is dropped from the refinement above 160 °C. In Figure 5, all the chemical transformations occur between 130 and 170 °C, which is consistent with prior results indicating more facile reduction of Cu in $\text{Ce}_{0.8}\text{Cu}_{0.2}\text{O}_2$ than in CuO.³³

The $\text{Ce}_{1-x}\text{Cu}_x\text{O}_2$ sample was then cooled to room temperature in the 5% H_2/He mixture and subsequently oxidized in a 5% O_2/He mixture as shown in the top of Figure 6 (25 → 400 °C, with a heating ramp of 4 °C/min). The corresponding Rietveld refinement results are shown in Figure 6b. At 90 °C, metallic Cu returned to the CeO_2 matrix to form a $\text{Ce}_{1-x}\text{Cu}_x\text{O}_2$ solid solution while passing through an intermediate Cu_2O phase. The kinetics of oxidation is much slower than that for reduction, with metallic Cu present until 230 °C when all Cu revealed by the

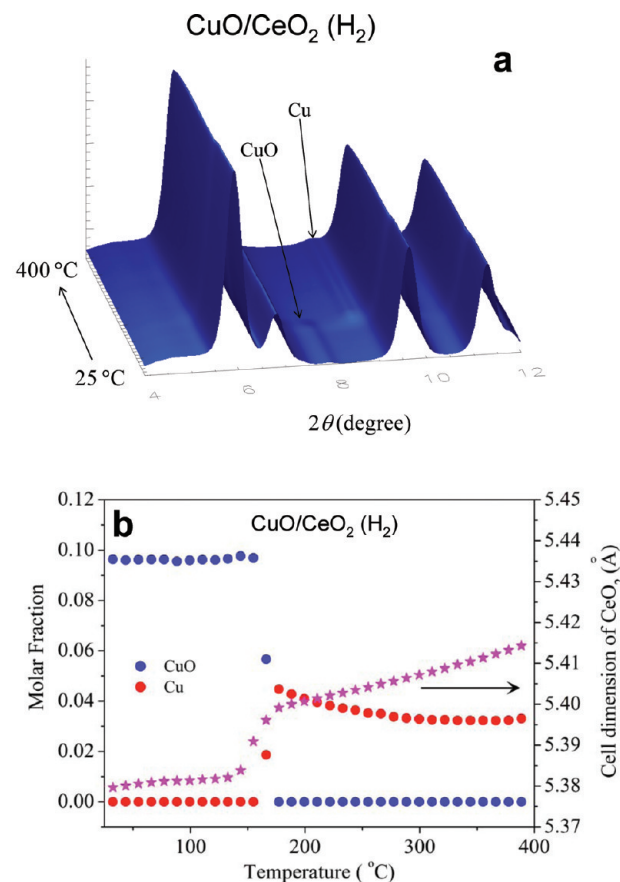


Figure 7. (a) *In situ* X-ray diffraction patterns collected during the heating of CuO/CeO_2 in 5% H_2/He from 25 to 400 °C at a heating rate of 4 °C/min. (b) Results of a Rietveld refinement for the *in situ* time-resolved XRD data. Cu content is plotted as the molar fraction of the Cu + Ce total.

Rietveld refinement has returned to the $\text{Ce}_{1-x}\text{Cu}_x\text{O}_2$ phase. However, the Cu:Ce ratio has reduced from 0.25 in the as-prepared material to 0.12 (0.11:0.89, obtained from Figure 6b) after the complete redox cycle. The remaining Cu, nearly 50% of the original content, has not crystallized into Cu, CuO , Cu_2O , or $\text{Ce}_{1-x}\text{Cu}_x\text{O}_2$ phases, suggesting either sublimation (unlikely at these experimental temperatures) or the presence of an amorphous phase (confirmed by ETEM). The absence of a discontinuity in the CeO_2 lattice parameter during heating suggests that oxygen vacancies are filled at room temperature with Ce returning to its full 4+ oxidation state long before the Cu is fully oxidized.

The full *in situ* redox cycle was identically repeated for the 5% CuO/CeO_2 sample. The XRD data for reduction in hydrogen are shown in Figure 7 together with the results of the Rietveld refinement. At room temperature, the as-prepared material contains no Cu dopant inside the CeO_2 phase. Upon heating to ~160 °C, one sees a direct $\text{CuO} \rightarrow \text{Cu}$ transformation (i.e., no formation of a Cu_2O intermediate) with a partial reduction of ceria (some $\text{Ce}^{4+} \rightarrow \text{Ce}^{3+}$) that produces an abrupt expansion of the lattice by 0.015 Å. This expansion is ~50% smaller than that seen in the experiments for the reduction of the $\text{Ce}_{0.8}\text{Cu}_{0.2}\text{O}_2$ solid solution, but the absence of Cu dopants for the CuO/CeO_2 case could explain this difference. During oxidation in 5% O_2/He , Figure 8, metallic Cu returns to the initial CuO phase through a Cu_2O intermediate not detected during reduction. The change in

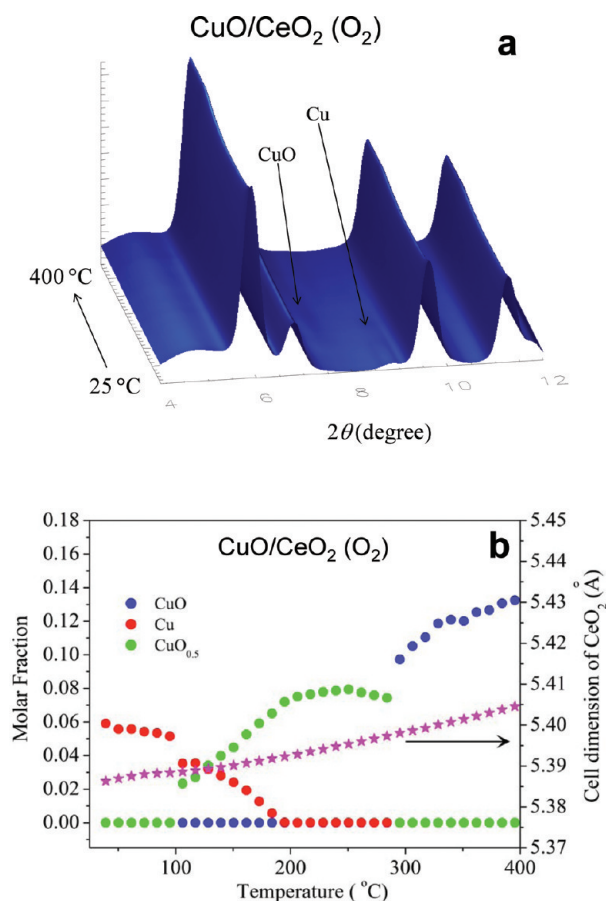


Figure 8. (a) *In situ* X-ray diffraction patterns collected during the reoxidation of reduced CuO/CeO₂ in 5% O₂/He from 25 to 400 °C at a heating rate of 4 °C/min. (b) Results of a Rietveld refinement for the *in situ* time-resolved XRD data. Cu content is plotted as the molar fraction of the Cu + Ce total.

lattice parameter during oxidation is again continuous, suggesting that reduced CeO₂ is largely reoxidized at room temperature. In the process of reoxidation for the reduced CuO/CeO₂ system, there was no incorporation of the copper into the ceria substrate and the formed CuO was crystalline. A comparison of the XRD results in Figures 6 and 8 points to the special properties of the reduced Ce_{0.8}Cu_{0.2}O₂ solid solution and its strong copper ↔ oxide interactions.

C. In Situ XANES Studies. To investigate the electronic structure of Cu-CeO₂ catalysts during a full redox cycle, *in situ* time-resolved Cu K-edge XANES were collected for the Ce_{0.8}-Cu_{0.2}O₂ and 5% CuO/CeO₂ materials. A previous study has discussed in detail the electronic transitions involved in the features present in the Cu K-edges of these samples.³⁴ The data for the Ce_{0.8}Cu_{0.2}O₂ nanocatalyst is displayed in Figures 9 and 10. The time-resolved reduction series displayed in Figure 9a indicates an onset of copper reduction at 150 °C, consistent with the depletion of copper seen for Ce_{0.8}Cu_{0.2}O₂ in the Rietveld refinement of the XRD data (Figure 5). By fitting the Cu XANES as a linear combination of native Ce_{0.8}Cu_{0.2}O₂ and metallic Cu, we note that the reduction is >90% complete at 175 °C. The corresponding reoxidation time series is displayed in Figure 9b and indicates that the Cu in reduced Ce_{0.8}Cu_{0.2}O₂ is 40% oxidized at room temperature but does not reach 90% until

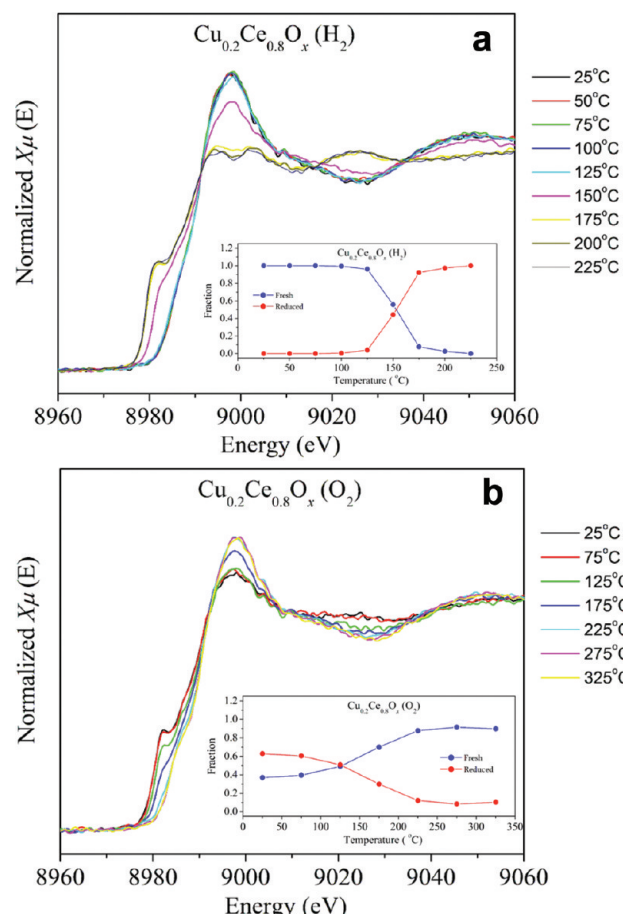


Figure 9. Effect of temperature on the *in situ* Cu K-edge XANES for Ce_{0.8}Cu_{0.2}O₂ during (a) reduction in 5% H₂/He and (b) reoxidation in 20% O₂/He.

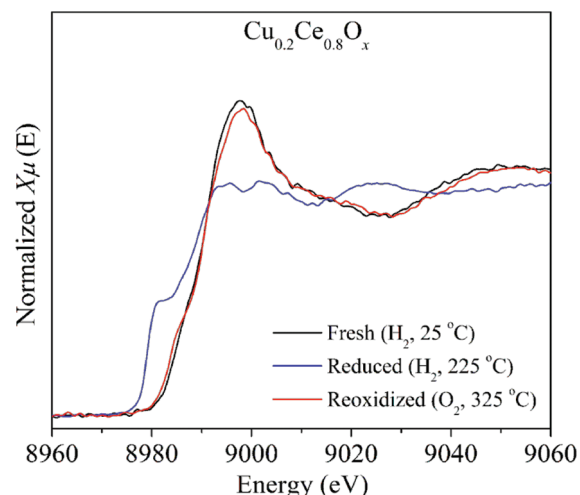


Figure 10. Comparison of the Cu K-edge line-shape of a Ce_{0.8}Cu_{0.2}O₂ sample fresh, after reduction in hydrogen, and after reoxidation with O₂.

225 °C. Rapid oxidation at room temperature agrees with the observation of an amorphous CuO_x phase by *in situ* ETEM which is presumed to be metastable. The XRD refinement shown in Figure 6b indicates that the reincorporation of Cu into the

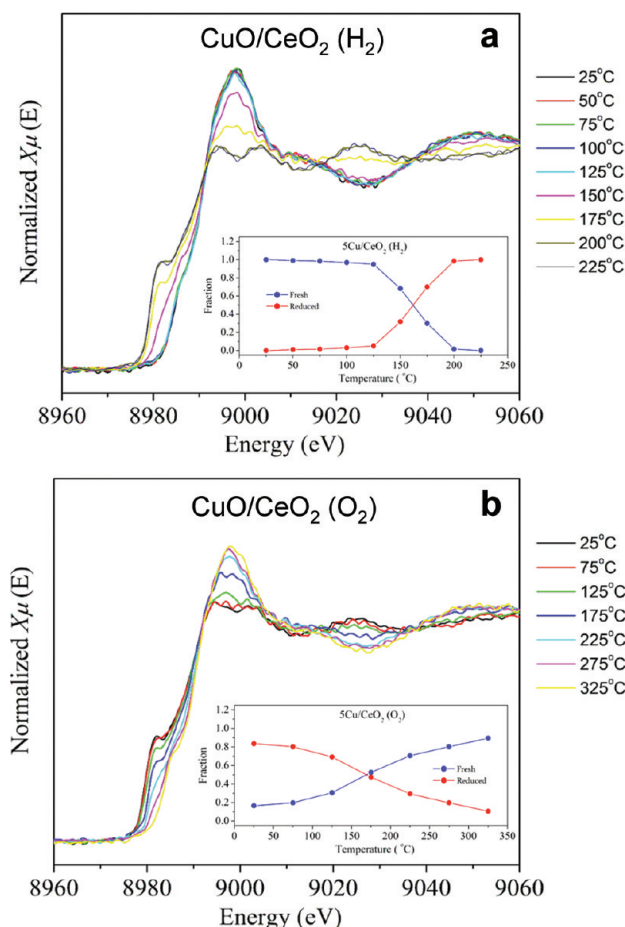


Figure 11. Effect of temperature on the *in situ* Cu K-edge XANES for 5% CuO/CeO₂ during (a) reduction in 5% H₂/He and (b) reoxidation in 20% O₂/He.

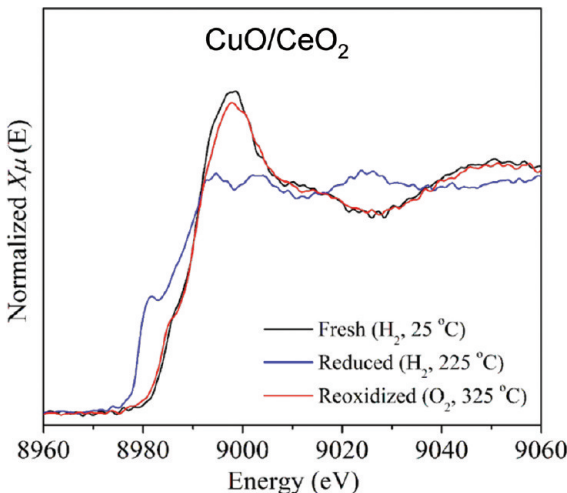


Figure 12. Comparison of the Cu K-edge line-shape of a 5% CuO/CeO₂ sample fresh, after reduction in hydrogen, and after reoxidation with O₂.

Ce_{1-x}Cu_xO₂ lattice occurs through a Cu₂O intermediate phase in the same temperature range of 100–225 °C where the remainder of Cu oxidation is observed by XANES. Figure 10

compares XANES spectra of the initial and final states of Ce_{0.8}Cu_{0.2}O₂ after one redox cycle. The remarkable similarity of the initial and final states of Ce_{0.8}Cu_{0.2}O₂ indicates that the oxidation state of Cu in the amorphous CuO_x seen in TEM is close to that of copper in Ce_{0.8}Cu_{0.2}O₂.

The time-resolved XANES reduction series from 5% CuO/CeO₂ is displayed in Figure 11a and indicates an onset of copper reduction at 150 °C, consistent with the depletion of CuO seen in the Rietveld refinement of the XRD measurements (Figure 7). Fitting the Cu XANES as a linear combination of native CuO/CeO₂ and metallic Cu reveals that the reduction is >90% complete at 200 °C, 25 deg hotter than required for Ce_{0.8}Cu_{0.2}O₂. This is consistent with the slower kinetics observed for reduction of the CuO/CeO₂ sample during *in situ* ETEM. The reoxidation time series is displayed in Figure 11b and indicates that the Cu in the reduced CuO/CeO₂ is 18% oxidized at room temperature but does not reach 90% until 325 °C, 100 deg hotter than required for Ce_{0.8}Cu_{0.2}O₂. Figure 12 compares XANES spectra of the initial and final states of CuO/CeO₂ after one redox cycle. As with Ce_{0.8}Cu_{0.2}O₂, the initial and final states are remarkably similar in their electronic properties.

SUMMARY AND CONCLUSIONS

Aberration-corrected environmental TEM, time-resolved XRD, and X-ray absorption spectroscopy were used to study *in situ* the structural, morphological, and electronic properties of Cu–CeO₂ nanocatalysts during reduction (using H₂) and oxidation processes (using O₂). We have found that both a Ce_{0.8}Cu_{0.2}O₂ solid solution and a CuO/CeO₂ blended system reduced to form a Cu/CeO₂ biphase with significant oxygen vacancies in CeO₂. In the case of the reduction of the Ce_{0.8}Cu_{0.2}O₂ solid solution, the formed Cu particles were smaller and better dispersed than those obtained upon reduction of the CuO/CeO₂ blended system. The smaller agglomeration of the Cu particles in reduced Ce_{0.8}Cu_{0.2}O₂ probably reflected stronger or more intimate copper ↔ ceria interactions. During subsequent *in situ* oxygen annealing, Cu precipitated from the CuO/CeO₂ blend reoxidized to form crystalline CuO through a Cu₂O intermediate, as expected. However, the Cu precipitated from the Ce_{0.8}Cu_{0.2}O₂ solid solution behaved rather differently under oxidizing conditions and neither oxidized to form crystalline CuO nor fully returned to yield the bulk phase of a Ce_{0.8}Cu_{0.2}O₂ solid solution. Rietveld refinement of powder diffraction data showed that 50% of the Cu returned to a Ce_{1-x}Cu_xO₂ solid solution, while the remainder was observed by *in situ* ETEM to form an amorphous CuO_x phase with a copper oxidation state similar to that of Ce_{1-x}Cu_xO₂, but with a local bonding environment similar to crystalline CuO. The behavior seen for the reduced Ce_{0.8}Cu_{0.2}O₂ points to strong interactions between copper and the ceria matrix and illustrates the advantages of utilizing solid solutions of mixed oxides.

ACKNOWLEDGMENT

This research carried out in part at the Center for Functional Nanomaterials and the National Synchrotron Light Source at Brookhaven National Laboratory, which are supported by the U. S. Department of Energy, Office of Basic Energy Sciences, under Contract DE-AC02-98CH10886. Thanks are due to Dr. Daniel Gamarra for the preparation of the samples. Financial support by MICINN (CTQ2009-14527/BQU) is acknowledged.

■ REFERENCES

- (1) Papavassilou, J.; Avgoustopoulos, G.; Ioannides, T. *Catal. Commun.* **2004**, *5*, 231.
- (2) Kung, H. H. *Transition Metal Oxides: Surface Chemistry and Catalysis*; Elsevier: New York, 1989.
- (3) (a) Park, S.; Vohs, J. M.; Gorte, R. J. *Nature* **2000**, *404*, 265. (b) Gorte, R. J.; Vohs, J. M.; McIntosh, S. *Solid State Ionics* **2004**, *175*, 1.
- (4) Klier, K. *Adv. Catal.* **1982**, *31*, 243.
- (5) Newsome, D. S. *Catal. Rev.* **1980**, *21*, 275.
- (6) Campbell, C. T. *Adv. Catal.* **1989**, *36*, 1.
- (7) Peppley, B. A.; Amphlett, J. C.; Kearns, L. M.; Mann, R. F. *Appl. Catal., A* **1999**, *179*, 31.
- (8) Reitz, T. L.; Lee, P. L.; Czaplewski, K. F.; Lang, J. C.; Popp, K. E.; Kung, H. J. *Catal.* **2001**, *199*, 193.
- (9) Dow, W.-P.; Huang, T.-J. *Appl. Catal., A* **1996**, *141*, 17.
- (10) Rodriguez, J. A.; Hanson, J. C.; Wen, W.; Wang, X. *Catal. Today* **2009**, *145*, 188.
- (11) PDF #41-0254, JCPDS Powder Diffraction File, Int. Center For Diffraction Data, Swarthmore, PA, 1989.
- (12) PDF #05-0667, JCPDS Powder Diffraction File, Int. Center For Diffraction Data, Swarthmore, PA, 1989.
- (13) O'Keeffe, M.; Bovin, J. O. *Am. Mineral.* **1978**, *63*, 180.
- (14) PDF #083-1665, JCPDS Powder Diffraction File, Int. Center For Diffraction Data, Swarthmore, PA, 2004.
- (15) O'Keeffe, M.; Moore, W. J. *J. Chem. Phys.* **1962**, *36*, 3009.
- (16) Huang, T. J.; Tsai, D.-H. *Catal. Lett.* **2003**, *87* (4), 173.
- (17) Wang, X.; Rodriguez, J. A.; Hanson, J. C.; Gamarra, D.; Martinez-Arias, A.; Fernandez-Garcia, M. *Top. Catal.* **2008**, *49*, 81.
- (18) Wen, W.; Jing, L.; White, M. G.; Marinkovic, N.; Hanson, J. C.; Rodriguez, J. A. *Catal. Lett.* **2007**, *113*, 1.
- (19) Rodriguez, J. A.; Kim, J.-Y.; Hanson, J. C.; Brito, J. L. *Catal. Lett.* **2002**, *82*, 103.
- (20) Nagase, K.; Zheng, Y.; Kodama, Y.; Kakuta, J. J. *Catal.* **1999**, *187*, 123.
- (21) Wang, J. B.; Tsai, D.-H.; Huang, T.-J. *J. Catal.* **2002**, *208*, 370.
- (22) Dow, W.-P.; Huang, T. J. *J. Catal.* **1994**, *147*, 322.
- (23) Martinez-Arias, A.; Fernandez-Garcia, M.; Gálvez, O.; Coronado, J. M.; Anderson, J. A.; Conesa, J. C.; Soria, J.; Munuera, G. *J. Catal.* **2000**, *195*, 207.
- (24) Severino, F.; Brito, J. L.; Laine, J.; Fierro, J. L. G.; López Agudo, A. J. *Catal.* **1998**, *177*, 82.
- (25) Dow, W.-P.; Huang, T. J. *J. Catal.* **1996**, *160*, 171.
- (26) Liu, W.; Flytzani-Stephanopoulos, M. *J. Catal.* **1995**, *153*, 317.
- (27) Fernández-García, M.; Rodríguez-Ramos, I.; Ferreira-Aparicio, P.; Guerrero-Ruiz, A. J. *Catal.* **1998**, *178*, 253.
- (28) Wang, X.; Rodriguez, J. A.; Hanson, J. C.; Gamarra, D.; Martinez-Arias, A.; Fernández-García, M. *J. Phys. Chem. B* **2006**, *110*, 428.
- (29) Liu, W.; Flytzani-Stephanopoulos, M. *J. Catal.* **1995**, *153*, 304.
- (30) Liu, W.; Flytzani-Stephanopoulos, M. *J. Catal.* **1995**, *153*, 317.
- (31) Qi, X.-M.; Flytzani-Stephanopoulos, M. *Ind. Eng. Chem. Res.* **2004**, *43*, 3055.
- (32) Shan, W. J.; Shen, W. J.; Li, C. *Chem. Mater.* **2003**, *15*, 4761.
- (33) Gamarra, D.; Munuera, G.; Hungría, A. B.; Fernández-García, M.; Conesa, J. C.; Midgley, P. A.; Wang, X. Q.; Hanson, J. C.; Rodriguez, J. A.; Martínez-Arias, A. *J. Phys. Chem. C* **2007**, *111*, 11026.
- (34) Wang, X.; Rodriguez, J. A.; Hanson, J. C.; Gamarra, D.; Martínez-Arias, A.; Fernández-García, M. *J. Phys. Chem. B* **2005**, *109*, 19595.
- (35) (a) Martínez-Arias, A.; Hungría, A. B.; Fernández-García, M.; Conesa, J. C.; Munuera, G. *J. Phys. Chem. B* **2004**, *108*, 17983. and references therein (b) Martínez-Arias, A.; Fernández-García, M.; Soria, J.; Conesa, J. C. *J. Catal.* **1999**, *182*, 367 and references therein.
- (36) (a) Wang, X.; Hanson, J. C.; Liu, G.; Rodriguez, J. A.; Iglesias-Juez, A.; Fernández-García, M. *J. Chem. Phys.* **2004**, *121*, 5434. (b) Wang, X.; Hanson, J. C.; Rodriguez, J. A.; Belver, C.; Fernández-García, M. *J. Chem. Phys.* **2005**, *122*, 154711.
- (37) (a) Fernández-García, M.; Martínez-Arias, A.; Guerrero-Ruiz, A.; Conesa, J. C.; Soria, J. *J. Catal.* **2002**, *211*, 326. (b) Iglesias-Juez, A.; Hungría, A. B.; Gálvez, O.; Martínez-Arias, A.; Fernández-García, M.; Conesa, J. C.; Soria, J. *Stud. Surf. Sci. Catal.* **2001**, *138*, 347. (c) Fernández-García, M.; Martínez-Arias, A.; Hungría, A. B.; Iglesias-Juez, A.; Conesa, J. C.; Soria, J. *Phys. Chem. Chem. Phys.* **2002**, *4*, 2473. (d) Hungría, A. B.; Martínez-Arias, A.; Fernández-García, M.; Iglesias-Juez, A.; Guerrero-Ruiz, A.; Calvino, J. J.; Conesa, J. C.; Soria, J. *Chem. Mater.* **2003**, *15*, 4309.
- (38) Wang, X. Q.; Hanson, J. C.; Frenkel, A. I.; Kim, J.-Y.; Rodriguez, J. A. *J. Phys. Chem. B* **2004**, *108*, 13667.
- (39) Hammersley, A. P.; Svensson, S. O.; Thompson, A. *Nucl. Instrum. Methods Phys. Res.* **1994**, *346*, 321.
- (40) (a) Larson, A. C.; von Dreele, R. B. GSAS General Structure Analysis System. Report LAUR 86-748, Los Alamos National Laboratory, Los Alamos, NM, 1995. (b) Rietveld, A. M. *J. Appl. Crystallogr.* **1969**, *2*, 65. (c) Toby, B. H. *J. Appl. Crystallogr.* **2001**, *34*, 210.
- (41) Newville, M.; Ravel, B.; Haskel, D.; Rehr, J. J.; Stern, E. A.; Yacoby, Y. *Physica B* **1995**, *208–209*, 154.